Michael P. Manahan, Sr.[1], Randall B. Stonesifer[2], Yang Soong[3], James M. Burger[4]

MINIATURIZED NOTCH TEST SPECIMEN AND TEST MACHINE DESIGN

REFERENCE: Manahan, M. P., Stonesifer, R. B., Soong, Y., and Burger, J. M., "Miniaturized Notch Test Specimen and Test Machine Design," Pendulum Impact Machines: Procedures and Specimens for Verification, ASTM STP 1248, Thomas A. Siewert and Karl Schmieder, Eds., American Society for Testing and Materials, Philadelphia, 1995.

ABSTRACT: Charpy V-notch specimens are widely used within the nuclear industry to monitor the effects of neutron damage to the reactor pressure vessel (RPV) beltline region. There is an ever-increasing need to obtain more notched bar impact data as plants age. Many plants will require more specimens for surveillance during the license renewal period. Other plants have experienced more embrittlement than originally anticipated, and it will be necessary to develop plant-specific Charpy shift trend curve models to ensure continued safe operation. Since physically based trend curves have not yet been validated, the use of plant-specific data will save the utilities operations costs since overly (arbitrarily) conservative models are no longer needed. Miniature specimens have also been used to characterize the material condition after vessel annealing. The use of miniaturized specimens which can be fabricated from previously tested full sized specimens offers one solution to this need for more fracture data.

Experiments performed using side-grooved miniaturized notch test (MNT) specimens have demonstrated that 1/16 scale miniature specimens can be designed to yield transitional fracture behavior and that the fracture appearance and energy-temperature curves can be quantitatively related to the conventional ASTM E23 specimen data. This paper presents the results of a study focused on designing an optimized MNT specimen and test machine. A combination of literature review, metallurgical analysis, and finite element analysis was used to consider such design parameters as minimum specimen cross-section, specimen length, notch acuity, the use of side grooves, side groove geometry, support span, and striker geometry. Two dimensional and three dimensional, elastic-plastic, large deformation, finite element analyses were used to compare stress/strain fields for standard and miniaturized specimens. Specimen and test machine geometries have been developed to ensure continuum requirements are met, the MNT specimen stress fields simulate those of the conventional specimen, and scatter for the miniature data is minimized.

[1]President, MPM Research & Consulting, 915 Pike Street, P.O. Box 840, Lemont, PA 16851

[2]President, Computational Mechanics, Inc., Rt. 2, Box 64, Julian, PA 16844

[3]Consultant, 6414 Terese Terrace, Jamesville, NY 13078

[4]Program Manager, ESEERCO, 1515 Broadway, 43rd Floor, New York, NY 10036

KEYWORDS: Charpy, miniaturized specimen testing, impact test, fracture appearance, lateral expansion, ductile-brittle transition temperature, upper shelf energy

---

INTRODUCTION

Neutron irradiation of nuclear reactor pressure vessel (RPV) materials results in embrittlement which must be accounted for in the fracture mechanics evaluation to determine Pressure-Temperature (P-T) operating limits. At present, the ASME K_{IR} curve is shifted by the Charpy V-notch (CVN) shift indexed at 41 J (ΔT_{41}) to account for neutron damage. Many plants require additional Charpy data to support license renewal, to provide plant-specific data, and, in several plants in Europe, to confirm the beneficial effects of vessel annealing. The use of miniaturized specimens which can be prepared from the broken halves of previously tested full sized specimens offers one solution to this need for additional data.

In the past, qualitative [1, 2, 3] interpretations of miniature Charpy data have been proposed to explain differences between the miniature specimen data and the ASTM E23 standard specimen results. The first successful quantitative interpretation of miniature Charpy data was reported in Reference [4]. The key elements of this approach are reviewed in the following section of this paper. The recently released ASTM STP 1204 [5] contains several papers focused on quantification of the miniature Charpy test [6, 7, 8, 9, 10]. Review of the work presented in References [5, 11] shows that there are presently widely differing miniature Charpy test approaches and data interpretations reported in the open literature. In support of miniature Charpy standardization work, a focused design study has been performed to optimize the miniaturized notched test (MNT) for nuclear RPV applications. The MNT is a dynamic three point bend test which has been designed to yield data which are quantitatively the same as those obtained in conventional Charpy testing. The key elements of this study are presented here. It is intended that the international standardization effort will lead to accepted standard practices related to miniature specimen geometry, test machine parameters, and data analysis. It is important to emphasize that the specimen size recommendations reported herein are only applicable to the U.S. RPV materials. Application to other classes of material must begin with an in-depth understanding of the material microstructure. The appropriate size and specimen geometry can then be determined using a similar approach.

BACKGROUND

Prior to performing a comprehensive design study, limited scope experiments were performed to demonstrate the feasibility of achieving transitional fracture behavior using specimens which are 1/16 of the volume of conventional Charpy specimens. These experiments have been reported in References [12, 4, 13, 14] and the key results are briefly discussed here.

An important limitation in miniaturizing any specimen is the extent of the material's microstructural inhomogeneities. The usual guideline dictates that the specimen be at least five to ten times as large as the characteristic heterogeneity dimension. Material for this work was taken from a special heat of ASTM A508 steel provided by Oak Ridge National Laboratory (ORNL) for crack arrest research as part of the Heavy Section Steel Technology (HSST) Program [15]. Microscopy

analysis indicated that carbon segregates in slender bands about 0.25 mm wide with a mean separation of 0.5 mm-1.0 mm. As a result of these findings, the minimum specimen cross section dimension was 5 mm.

Early MNT static tests demonstrated that 1/16 volume miniature Charpy specimens, when tested in the transition region or upper shelf, yield data which cannot be properly analyzed nor related to conventional Charpy data (severe nonplanar fracture surfaces were observed). These nonplanar failures in the miniature specimens were due to their plastic collapse load being smaller than their fracture load. This behavior is consistent with the well known tendency for smaller fracture specimens to behave in a more ductile manner than larger specimens of similar geometry. This behavior is basically due to the fact that stress intensity factors scale with the square root of the specimen size. For example, a half scale specimen will require about 1.41 (i.e., $\sqrt{2}$) higher applied stress than a full scale specimen to achieve the same stress intensity factor level. This behavior was perhaps exaggerated in these miniature specimens due to their very short lengths resulting in relatively larger shear stress to bending stress ratios than found in proportionally scaled specimens. This failure mode problem was overcome by adding side grooves to the specimens. The side grooves offset the loss of constraint associated with the increase in plastic deformation and stress levels to achieve fracture in the smaller specimens.

As discussed in Ref [4], either percent shear or percent post maximum load energy (PMLE) can be used as valid MNT parameters. However, it is essential that the ductile-to-brittle transition temperature (DBTT) be determined using an index which accurately represents the actual fracture process. In particular, for a given index, the fracture mode in the miniature specimen should be identical to that in the conventional specimen. Therefore, tracking embrittlement using percent shear data obtained from miniature specimens is ideal. Since the regulations within the nuclear industry are based on the 41 J index with absorbed energy as the parameter, the PMLE is preferable since it can be related directly to the conventional specimen absorbed energy. Figure 1 provides the correlation for obtaining these indices for both specimen dimensions for A508 steel. This technique can be used to relate any specimen geometries that yield notched specimen fracture transition data. For example, for the A508 steel used in this study, a Charpy energy level of 41 J corresponds to about 4% shear fracture appearance in the unirradiated condition. Referring to Fig. 1, this level of shear corresponds to about 15% PMLE. Thus, when fracture appearance is used as the MNT parameter, the corresponding index is 4% shear for this particular steel. When PMLE is chosen as the MNT parameter, a value of 15% PMLE is used as the index. Either index accurately tracks the miniature specimen Charpy shift at 4% shear and will provide 41 J Charpy shift data which is identical to the conventional specimen ΔT_{41}.

On comparing the miniature and conventional DBTTs, correction factors due to rate effect and size effect were obtained. The average shift due to rate effect for the conventional CVN is 45.3°C. This shift was determined by averaging the static to dynamic shift at the 41-J level for the three materials using conventional Charpy specimens. This is in reasonable agreement with the correlation presented in Ref. [16]. These data can be used to relate the MNT data with conventional, dynamic Charpy data for the ASTM A508 steel. The dynamic 41-J transition temperature is obtained by adding the rate effect shift (45.3°C) and the size effect shift (21.3°C) to yield a 41-J dynamic conventional Charpy transition temperature. Based on the successful experimental feasibility demonstration, an in-depth experimental design study was performed to develop appropriate size ranges for key parameters in the MNT.

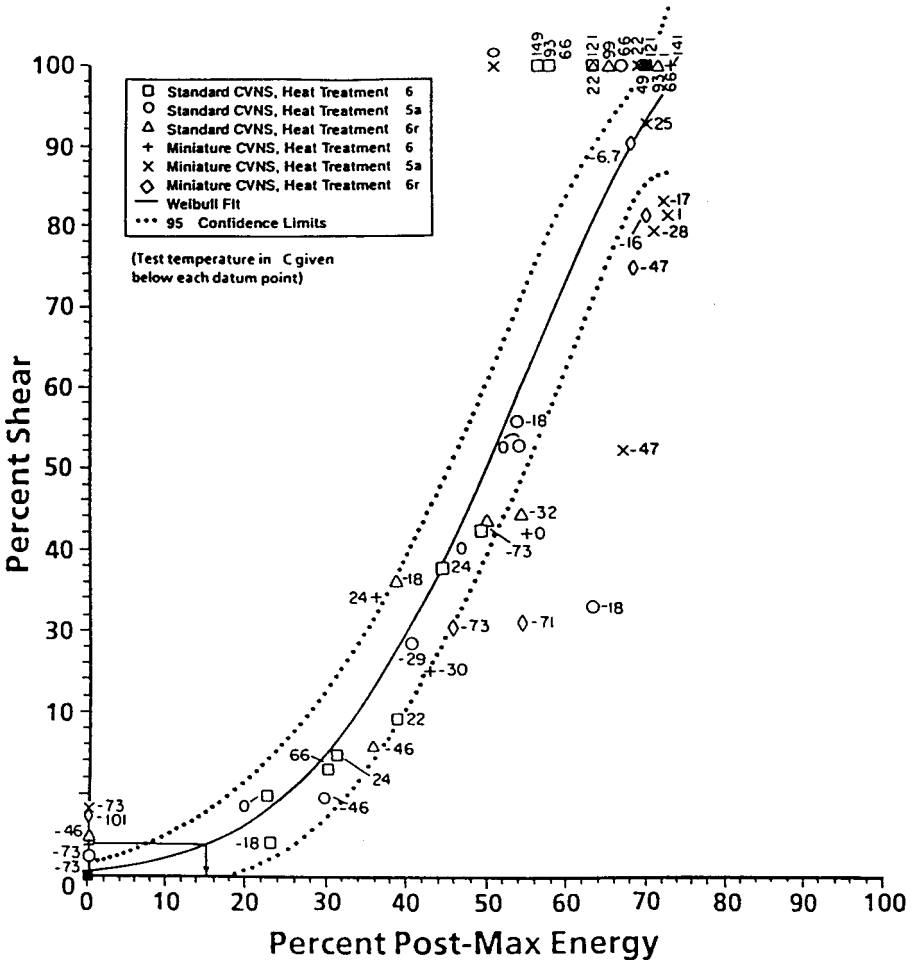

FIG. 1--Percent PME as a fracture transition criterion (miniature and standard specimen sizes)

MNT EXPERIMENTAL DESIGN

Miniature Specimen Cross Section

It is, of course, possible to perform an in-depth microstructural study for each material for which a miniaturized Charpy test is conducted. However, a more effective approach would be to define a specimen size which is adequate for determining MNT properties for a defined class of materials. This latter approach has been pursued and will form the basis for recommendation to the standards committees.

To adequately sample a representative volume of an RPV steel when using MNT specimens, one must know the scale, or mean separation, of the inhomogeneities that exist in the steel plate from which the pressure vessel is fabricated. The term inhomogeneity as used here refers to such compositional and microstructural characteristics as: solute segregation during solidification which leads to bands of variation in mean chemical composition and stringers of inclusions; grain boundaries (grain size); colonies of transformation products; precipitates; and the presence of Fe and alloy carbides. The scale of the inhomogeneities depends upon both compositional and processing variables. Base, weld, and heat-affected zone (HAZ) materials were analyzed for the U.S. vessel steels to determine the cross sectional dimensions which will ensure adequate material sampling. This analysis was performed to provide a conservative estimate of the minimum MNT specimen cross sectional dimensions so that microstructural measurements are not required for each heat of nuclear reactor pressure vessel material tested.

Base Plate--The size scale of various microstructural features considered for U.S. RPV steels are shown in Table 1. It is concluded that the coarsest inhomogeneity in the base plate is chemical banding that occurs especially in high-Mn steels. The variation in Mn content across the banding leads to the formation of a range of transformation products, and thus a range of properties throughout the plate cross section. Therefore, the band separation will be the factor which controls minimum specimen size in RPV plates. An approximate relation for the spacing of bands (L) based on the casting size and the total reduction from ingot to plate is: $L = 0.116\ \theta_f$ (mm), where θ_f is the

TABLE 1--Size scale of various microstructural features in reactor pressure vessel steels

Inhomogeneity Type	Scale (mm)
Chemical banding	0.5-1
Inclusion stringers	~0.5
Austenite grain size (TE)	0.06-0.2
Ferrite grain/pearlite colony size	0.01-0.08
Bainite/martensite colony size	~0.05
Carbide spacing in	
pearlite	0.0001-0.005
bainite	~0.002
martensite	≤0.0001

plate thickness (expressed in inches) [17]. Accordingly, high-Mn RPV plates which are typically 4 to 10 inches thick are predicted to contain chemical bands with an average separation of 0.5 to 1.1 mm. Observations on a section of forged A508 plate confirm these predictions [14]. Stringers of inclusions, which are concentrated in the chemical bands, are the next coarsest inhomogeneity in RPV plate. The primary effect of inclusions (sulfides, oxides, oxy-sulfides) is a loss of ductility (manifested as a decrease in the upper shelf energy (USE)) because of the weakness of the interface between metal and inclusion, and because of the brittleness of the inclusions. The separation of inclusion stringers is somewhat finer than that of the bands since the stringers can form at any point within the rather diffuse band width. Thus, tensile and Charpy specimens designed to sample a volume that will include chemical banding will of necessity include an adequate sample of inclusion stringers.

Other chemical and microstructural inhomogeneities in the plate are on a finer scale than either the bands or stringers and thus will be adequately sampled by specimens designed to include the coarser inhomogeneities. Accordingly, the cross sectional dimension of mini-specimens cut from base plate, assuming that five times the coarsest inhomogeneity will provide an adequate sampling, will be dictated by the banding separation which varies with plate thickness. From the above analysis, specimen cross sections will range from 2.5 mm for 4-inch plate to 5 mm for 10-inch plate.

HAZ--Throughout most of the HAZ, there is no massive redistribution of solute during the very short dwell time at high temperature experienced during the weld thermal cycle. Austenite grain size in the coarse grain HAZ (CGHAZ) may approach 0.5 mm in plates of all thicknesses depending on heat input and peak temperature. Thus the scale of temper embrittlement (TE) may be on the same order as the banding (~0.5 mm), and would therefore require specimens taken from the CGHAZ to have a cross section dimension of at least 2.5 mm. Therefore, the spacing of chemical banding present in the base plate (0.5-1 mm) still remains the controlling factor in determining the cross sectional dimension of mini-specimens cut from the HAZ.

Weld Bead--In the weld bead the grain structure is columnar, the width of the columns being 0.2-0.5 mm. In addition, centerline segregation of impurities often occurs. Specimens should therefore be notched at the centerline and have a cross section dimension on the order of 2.5 mm or greater.

Miniature Specimen Length

Based on microstructural considerations, miniature Charpy specimens cut from RPV materials should have minimum cross sectional dimensions of 5 mm x 5 mm, unless a smaller size can be justified by thorough microstructural characterization. Using the scale factor of 1/2 that was selected for designing the miniature specimen cross-section to select the specimen length would allow 8 miniature specimens (each 27.5 mm long) to be fabricated from the material of one standard Charpy specimen. The experimental work described earlier used specimens with half of this scaled length and therefore allowed 16 miniature specimens (each 13.75 mm long) to be obtained from the material of one standard specimen. Although the experimental data showed good characterization of the transitional fracture behavior, it is not clear that the stress field of the 13.75 mm long miniature specimen adequately simulates that of the conventional specimen. Therefore, the bending-to-shear stress ratio analysis described below was performed to determine the optimal specimen length.

In discussing the effect of length on specimen behavior, it is convenient to refer to the bending-to-shear stress ratio. This is just the ratio of the nominal peak bending stress to the shear stress that results from a simple strength of materials analysis of a smooth bar with the same overall dimensions as the fracture specimen. For simply supported rectangular bars, the bending-to-shear stress ratio is 3S/D, where S is the distance between supports, and D is the specimen depth. For the standard Charpy specimen, the ratio is 12. For the 1/16 volume miniature specimens [4], the ratio is 7.1. Proportional scaling of cross-sectional dimensions and length by a factor of 1/2 results in the scaled specimen having the same ratio as the standard Charpy specimen.

If the bending-to-shear ratio is sufficiently large, then the form and intensity of the notch and subsequent crack tip fields are effectively determined by the applied bending moment. For smaller specimen span-to-depth ratios, the load required to achieve a given bending moment is increased. For a four point loaded specimen, these larger loads would tend to be of little consequence since the notch region would be under pure bending and the stress and strain concentrations around the load points would be remote to the fracture plane. For the three point bending configuration of the Charpy specimen, however, the striker contact region stress field and associated plastic zone can begin to interact with that of the notch (or crack) if the load levels are sufficiently large. Decreasing the specimen span-to-depth ratio would result in such interaction effects occurring at a lower applied moment. Even with the same span-to-depth ratio, a smaller specimen will require a larger applied load (relative to the yield load for example) than a full scale specimen to achieve the same applied J level. Therefore, even with the same span-to-depth ratio, the interaction between the notch/crack tip fields and the tup contact related fields will occur at a lower level of crack field intensity for the smaller specimen. Using a smaller span-to-depth ratio in a smaller specimen would just compound this undesirable behavior.

The tendency for the miniature specimens that were used in previous studies to fail outside the intended fracture plane when side grooves were not used could have been increased by using a smaller bending-to-shear ratio. The failure of these specimens apparently involved plastic slip along the plastic zone that resulted from the notch region plastic zone linking up with the plastic zone formed in the tup contact region. The contact stresses for a given moment and notch/crack field intensity would have been larger due to the decreased span-to-depth ratio. This would result in correspondingly more intense contact region plastic zones. Another contributing factor to this undesirable failure mode would be the increased level of average shear stress acting in the region where the plastic zones link (average shear stress on the section is proportional to the applied load). This shear stress would tend to promote the type of slip that resulted in the observed failure mode.

As the above discussion shows, the only benefit to using a shorter specimen is the ability to get more miniature specimens from a given amount of material. Since it seems likely that weld reconstitution will allow the benefits of a smaller length (i.e., more specimens), while still allowing the benefits of a proportionately scaled standard specimen, a scale factor of 1/2 was recommended for designing the miniature specimen length.

The Plane Strain Nature of 3D Notch Region Stresses

To determine the degree to which the 3D notch region stresses are plane strain in nature, the stress distributions in the fracture plane were compared to the 2D plane strain solution. The ABAQUS general

purpose non-linear finite element code was used to perform these calculations. A typical finite element mesh and coordinate system are shown in Figure 2. Eight-noded brick elements were used in the analysis and finite strain theory was included in all calculations. The material flow curve was idealized as piece-wise linear. In the discussion which follows, general yield load is defined as the load at which yielding has spread across the entire uncracked ligament. This load corresponds to the "knee" in the load-deflection curve. In the cases where side-grooves were analyzed, a 45 degree included angle was modelled with 20% depth.

Figures 3 through 5 show the notch region stress field comparisons for the three applied displacement levels of 0.2 (near general yield), 1.5, and 3.0 mm (near peak load). In order to determine the dependence of the behavior on position along the notch front, stresses from the 3D midplane (solid line) are plotted as well as stresses from a position about half way between the midplane and the surface plane (dashed line).All three normal stress components are plotted in addition to the hydrostatic stress. The hydrostatic stress is the average of the three normal stresses and is considered to be an effective measure of constraint.

Figure 4 compares the 2D and 3D fracture plane stress distributions at a displacement of 1.5 mm which is about 8 times the displacement at general yield. At this load level, the peak σ_{yy} stresses occur at about 2.5 times the initial notch root radii from the notch surface. Except for the effect on the through thickness stress (σ_{zz}), the increased plasticity associated with this load level has led to very little loss of plane strain behavior compared to that at general yield. To the extent that the hydrostatic stress behavior is believed to be a more important measure of plane strain behavior than the through thickness stress, it can be reasonably argued that the center half of the 3D specimen notch fronts are still predominately plane strain. At this load level, the side grooves are again seen to provide an improvement of the σ_{zz} distributions.

Figure 3 compares the 2D and 3D fracture plane stress distributions for a full size standard specimen at about the general yield load. The stress distributions are plotted versus the distance from the notch tip, where the notch tip is normalized by the original notch tip radius (0.25 mm). The portion of the stress distribution important to fracture behavior is that between the notch tip and the peak stress (σ_{yy}) location. For this load level, the peak stress location is about 1.5 notch root radii from the notch surface. At least the center half thickness of both 3D geometries (with side grooves and without) is very near to plane strain conditions. At this load level, even the through thickness stress (σ_{zz}) is very close to that of the 2D plane strain solution. The side grooves provide a slight improvement of the σ_{zz} distribution at the intermediate plane.

Figure 5 compares the 2D and 3D fracture plane stress distributions at a displacement of 3.0 mm which is about 15 times the displacement at general yield. At this load level, the peak σ_{yy} stresses occur at about 3.5 times the initial notch root radii from the notch surface. The "bump" in the σ_{yy} stress distributions near the notch surface is believed to be the result of excessive distortion in the finite elements near the notch tip. To the extent that the element distortion affects the 2D and 3D solutions similarly, it is believed that this numerical anomaly does not impact the conclusions to be drawn from these solutions. Again, except for the effect on the through thickness stress (σ_{zz}), the increased plasticity associated with this load level has led to very little loss of plane strain behavior at the examined sections. The improvement in the σ_{zz} stress distribution for the side grooved specimen at higher loads is apparent in Figure 5. The

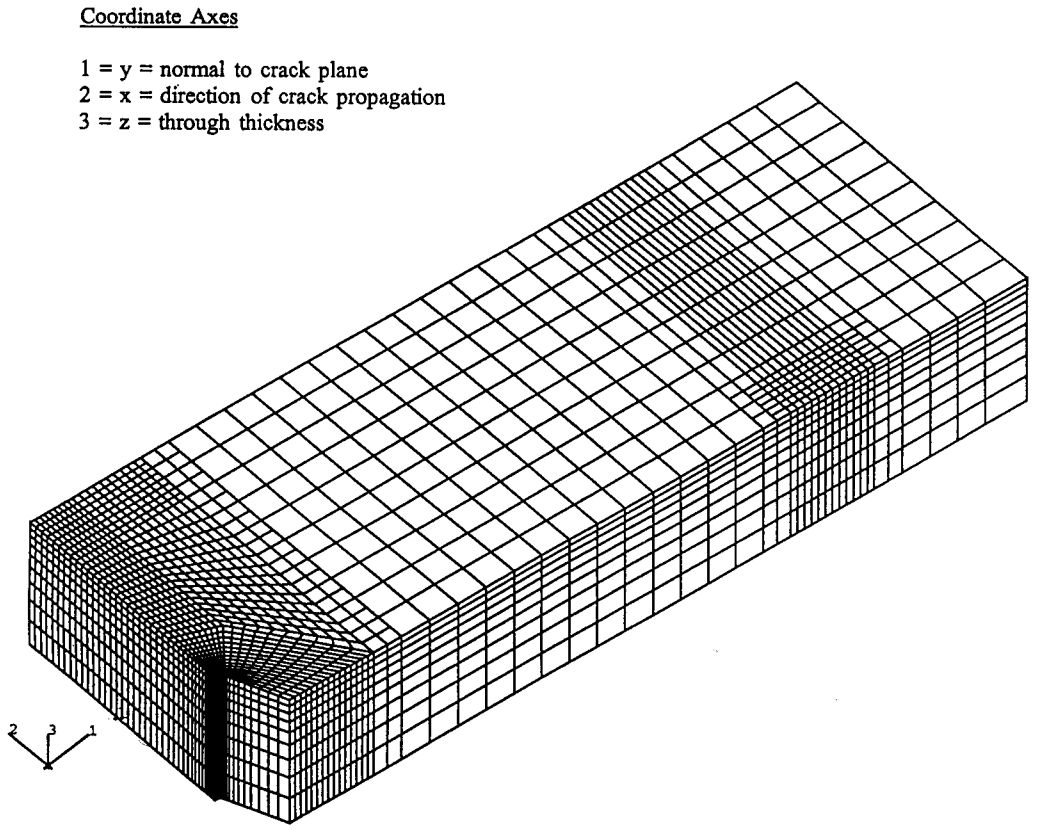

FIG. 2--Refined 3D finite element grid of the standard Charpy specimen

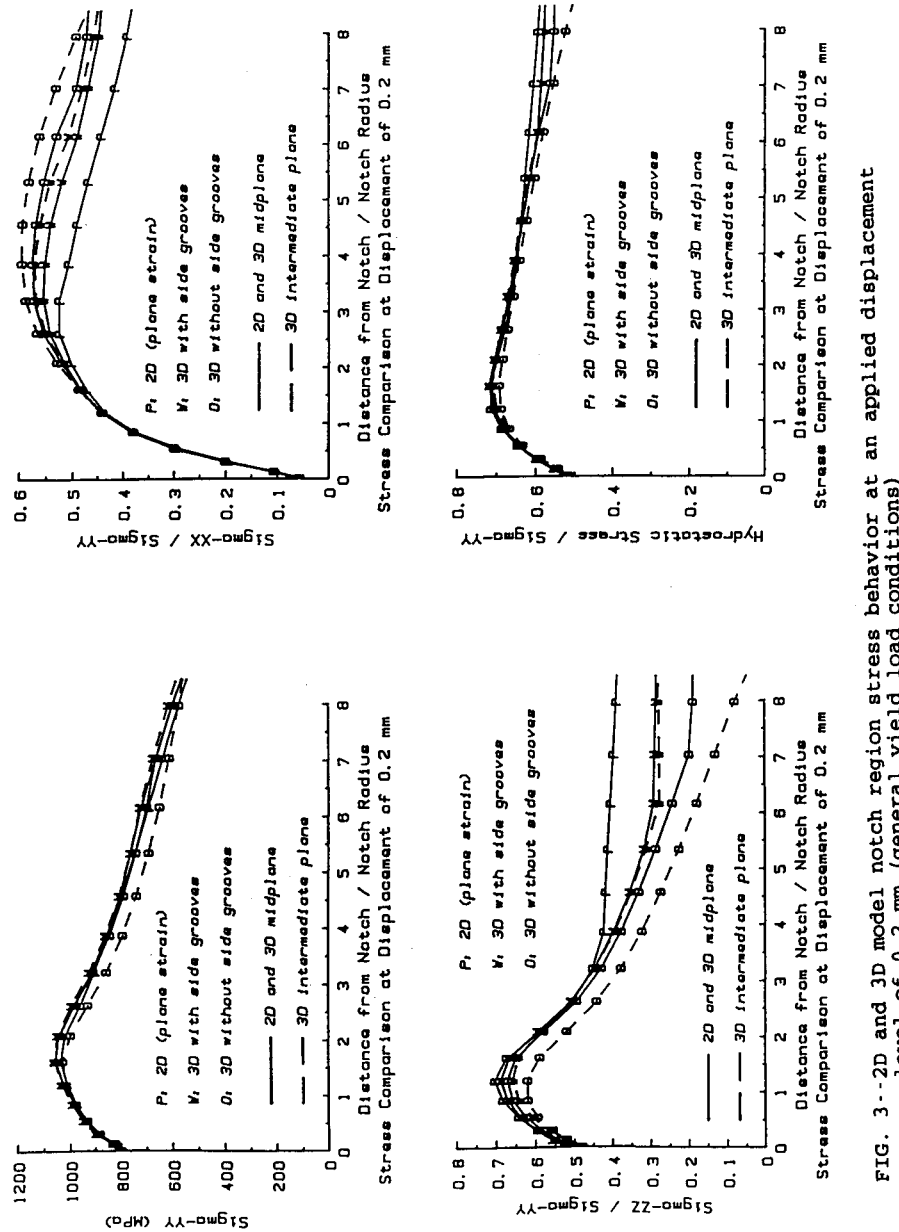

FIG. 3--2D and 3D model notch region stress behavior at an applied displacement level of 0.2 mm (general yield load conditions)

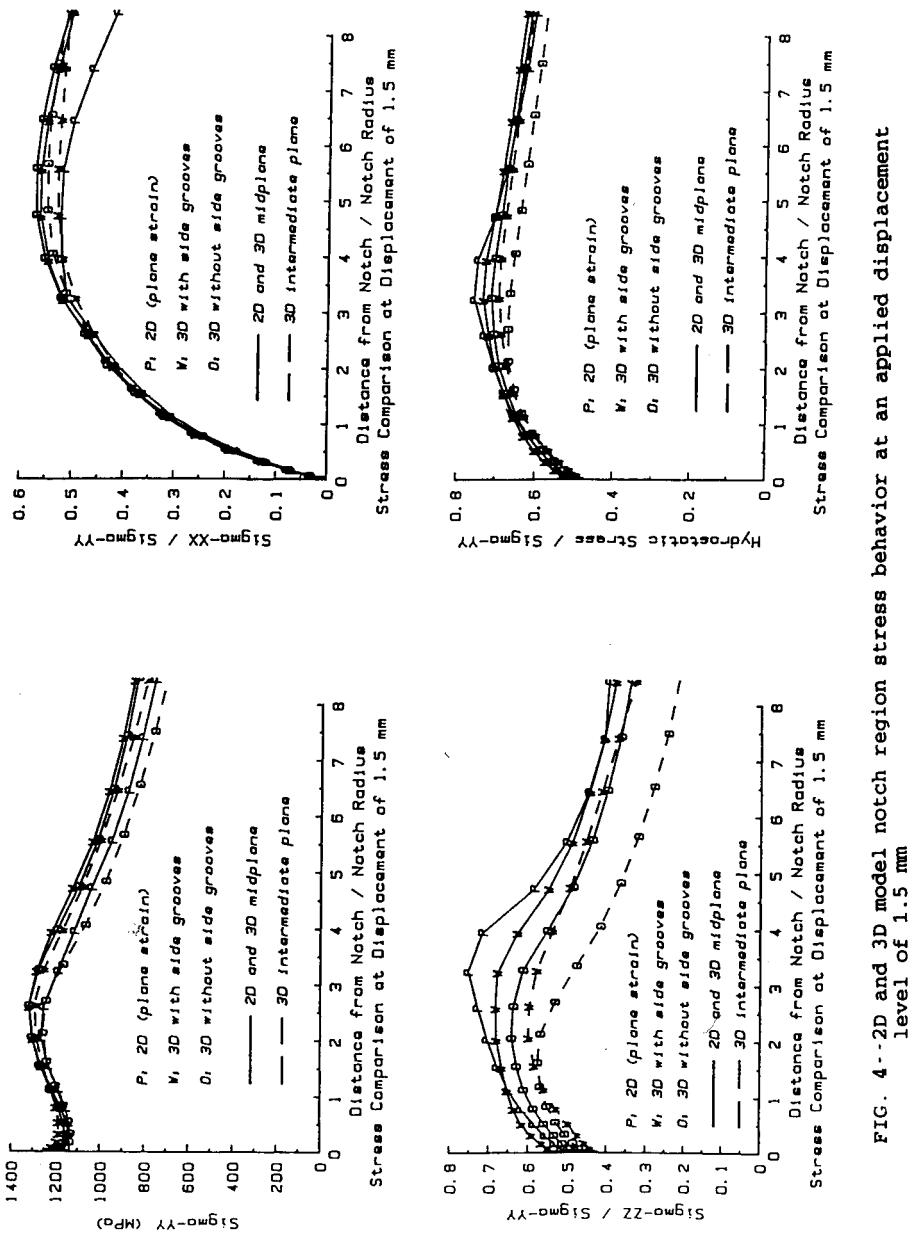

FIG. 4--2D and 3D model notch region stress behavior at an applied displacement level of 1.5 mm

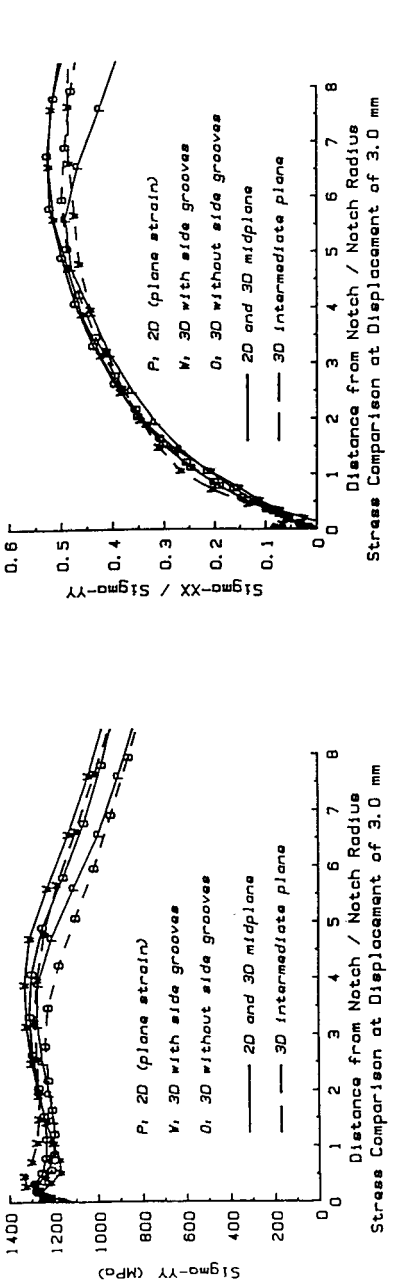

FIG. 5--2D and 3D model notch region stress behavior at an applied displacement level of 3.0 mm (near peak load conditions)

3D side groove solution behavior at small distances from the notch seen for the σ_{zz} stress is believed to be the result of the relatively coarse side groove modeling contributing to the above noted element distortion effects.

In summary, it can be concluded from the finite element solutions that the center-half portions of the notch fronts for side grooved and non-side grooved specimens exhibit plane strain behavior for applied displacement levels up to those representative of general yield. Beyond general yield load, the through thickness stresses are much closer to plane strain when the specimen is side grooved. Further comparisons using stress contours on the fracture plane will be made below. The beneficial effect of the side grooves will become more apparent during that discussion.

Central Notch Region Stress Behavior

The relevance of the 2D plane strain idealization to the central notch front region stress states has been demonstrated. In this section stress behavior from a refined 2D plane strain model are presented. Contours of the $\sigma_{yy}(=\sigma_{11})$ stress in the notch tip region for an applied displacement of 3 mm showed that this stress component peaks on the notch symmetry plane at a point that is about 2.5 times the initial notch radius or about 1 times the deformed notch radius. Severe distortion of the elements at the notch tip was observed. The σ_{xx} $(=\sigma_{22})$ stress component is zero at the notch tip and peaks at about 4 times the initial notch tip radius from the notch tip. The $\sigma_{zz}(=\sigma_{33})$ also peaks ahead of the notch tip. Contours of equivalent plastic strain, unlike the stress contours, show that the peak plastic strain occurs at the notch tip surface. The plastic strain gradient is very large near the notch tip. The hydrostatic stress peaks at about 4 times the initial notch root radius for this load level.

Stresses at the notch symmetry plane as functions of distance from the notch tip were analyzed at four load levels. The lowest load level is 0.63 of the Green & Hundy (G&H) [18] general yield load (P_o) and therefore has very limited plasticity effects. The highest load level that was analyzed is for a load ratio of 1.56. The (σ_{yy}) stresses tend to peak at 1 to 3 initial notch tip radii from the notch tip surface. Also, the distance to the peak stress increases with load level as is predicted by the G&H model. Since these results are from a large deformation finite element formulation, this shift is probably amplified due to the fact that the notch tip radius is increasing as the load increases. As with σ_{yy}, the location of the peak values of the σ_{xx} and σ_{zz} stresses is shifted further from the notch tip with increasing load, and again there is an apparent change in the near tip stress behavior between the 1.27 and 1.56 load levels which is probably due to severe finite element distortion at the notch tip. Figure 6 shows the hydrostatic stress behavior using two normalizations. It can be seen that the hydrostatic stress behavior changes in going from a largely elastic notch tip field (P/P_o = 0.63) to a largely plastic field (P/P_o = 1.02). Considering that higher hydrostatic stresses indicate higher constraint, it can be seen that plasticity initially increases constraint near the notch tip while lowering it at locations farther from the notch tip. Then further plasticity causes the location of the highest constraint to move farther from the notch tip. Using the σ_{yy} normalization, it can be seen that once the yield load is exceeded, the magnitude of the peak constraint increases, but only by a small amount.

Side Groove Effects on Notch Region Stress Behavior

Putting side grooves in the MNT specimens has two fundamental effects. By reducing the fracture plane area, the load required to achieve a critical stress state is reduced. At the same time, the

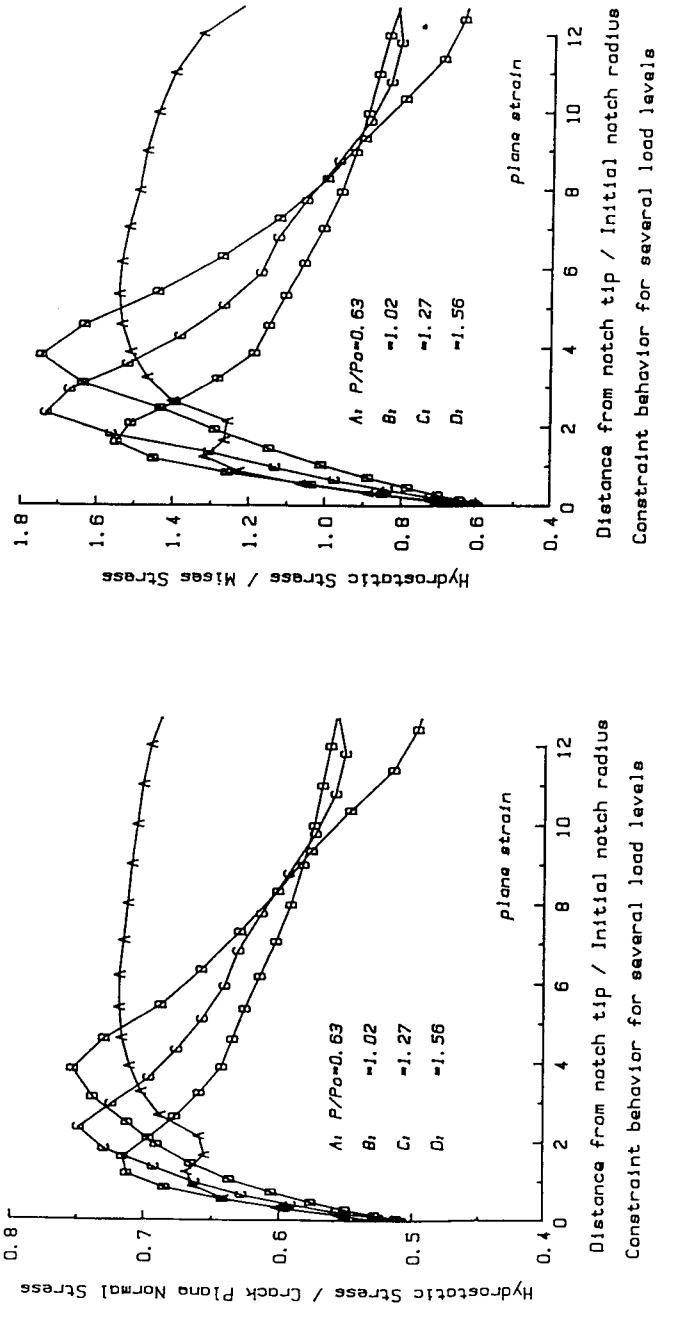

FIG. 6--Notch tip region behavior of hydrostatic stress at four load levels (refined 2D plane strain model of the standard Charpy specimen)

cross-section at the region where plastic collapse can occur in the non-side grooved specimens is not reduced. Therefore, the shear stress in the plastic zone to either side of the fracture plane is significantly reduced by the addition of side grooves. This results in an increase in the plastic collapse load relative to the fracture load. The second fundamental effect, as will be demonstrated in the following discussion, is that a larger portion of the notch front has plane strain fields.

In the following, crack plane stress fields from the 3D models of a standard Charpy specimen and a standard specimen with 20% side-grooves are compared. The purpose of the comparison is to show how the introduction of side grooves affects the variation in stress field behavior in going from the specimen midplane to the external specimen surface. Since the crack plane normal stress (σ_{yy}) and the hydrostatic stress are considered to be the most important stress quantities for illustrating plane strain behavior, only these stresses are compared.

Figures 7 through 10 compare the crack plane σ_{yy} and hydrostatic pressure contours for the refined 3D model with side grooves and the refined 3D model without side grooves. Figures 7 and 8 show the behavior at a displacement of 0.2 mm (approximately at general yield), and Figures 9 and 10 show the behavior at 1.5 mm of displacement. The left side plots in these figures are the results without side grooves and those on the right are with 20% side grooves. The notch front is the right edge of each contour plot while the left edge is at the tup contact region. The bottom edge of these plots corresponds to the specimen midplane. For the model without side grooves, the top edge of the plot is the external surface of the specimen. For the model with side grooves, the top edge of the plot corresponds to the root of the side groove.

In Figures 7 and 8 it can be seen that there is a significant reduction in the σ_{yy} and hydrostatic stress between the quarter thickness plane (intermediate plane of Figures 3, 4, and 5) and the external surface of the specimen. For the side grooved specimen, the stresses near the notch show little variation between the midplane and the side groove root. Since Figure 3 shows that both 3D models have plane strain behavior at the midplane, it can be concluded, that adding side grooves resulted in an increase in the portion of the notch exhibiting plane strain behavior. In Figures 9 and 10, it can be seen that the loss of plane strain behavior over the outer quarter thickness of the model without side grooves is greater than it was for the smaller displacement level. Although there is some reduction in the hydrostatic stress for the side grooved specimen near the side groove, the loss is much less significant than for the model without side grooves. Calculations at 3 mm of displacement showed that the loss in plane strain behavior in the outer quarter thickness of the side grooved and non-side grooved models is not substantially different than at the displacement level of 1.5 mm. This strongly suggests that further displacement increases would not result in substantially different plane strain behavior than observed at 1.5 and 3 mm of displacement.

The observation that the loss of plane strain behavior does not appear to continue after a displacement of about 8 times the general yield displacement is important. This is because dimensional analysis shows that miniature specimens will require relatively larger displacements than full scale specimens to achieve comparable crack tip field intensities. Further, the use of side grooves results in a larger volume of material being sampled at near plane strain conditions. We estimate that for the miniature specimen with side grooves the peak hydrostatic stress field extends along the notch to 80% of the distance calculated in the conventional specimen. Whereas, the peak hydrostatic

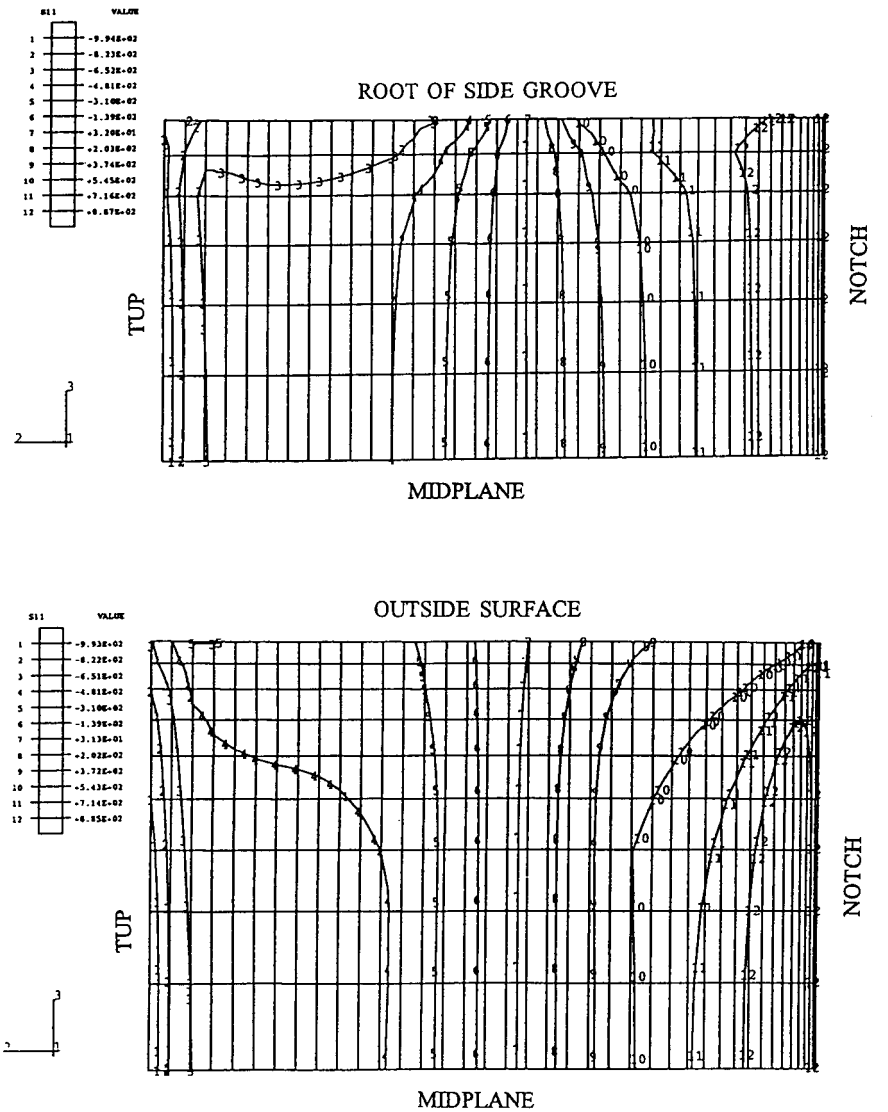

FIG. 7--Comparison of fracture plane σ_{yy} contours at a displacement of 0.2 mm for notched specimens both with (top) and without (bottom) side grooves

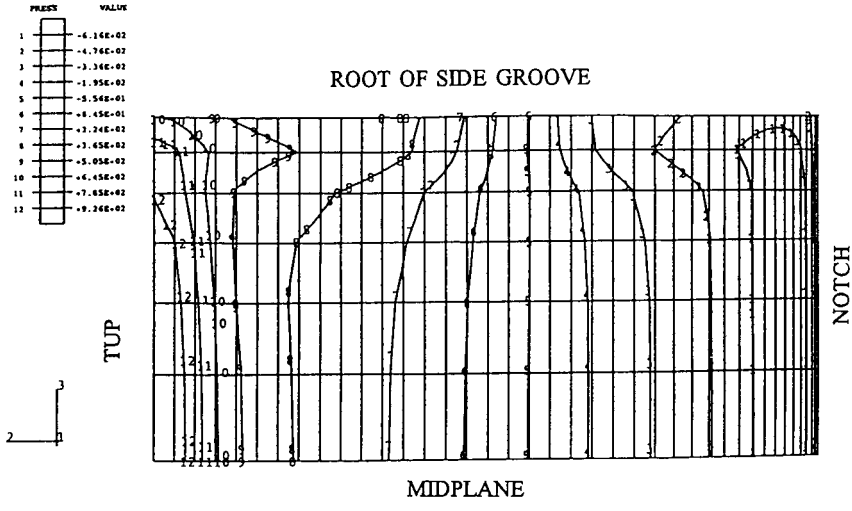

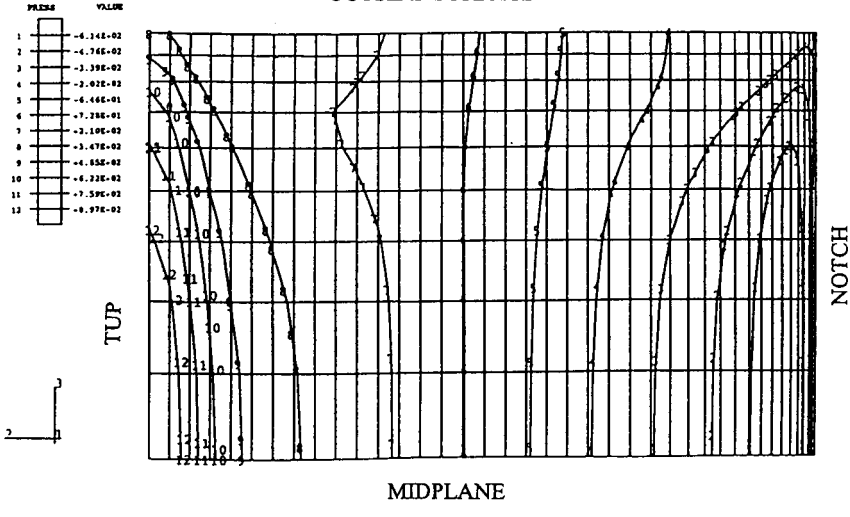

FIG. 8--Comparison of fracture plane hydrostatic pressure contours at a displacement of 0.2 mm for notched specimens both with (top) and without (bottom) side grooves

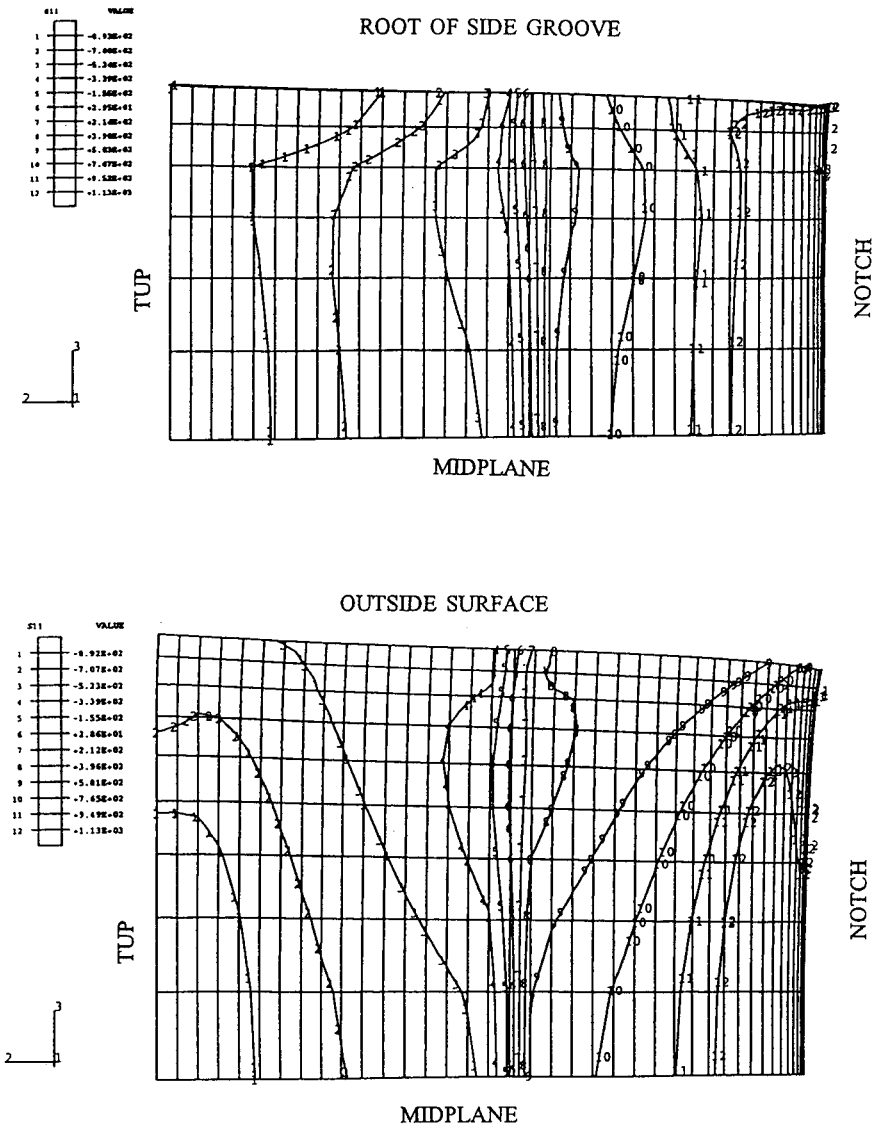

FIG. 9--Comparison of fracture plane σ_{yy} contours at a displacement of 1.5 mm for notched specimens both with (top) and without (bottom) side grooves

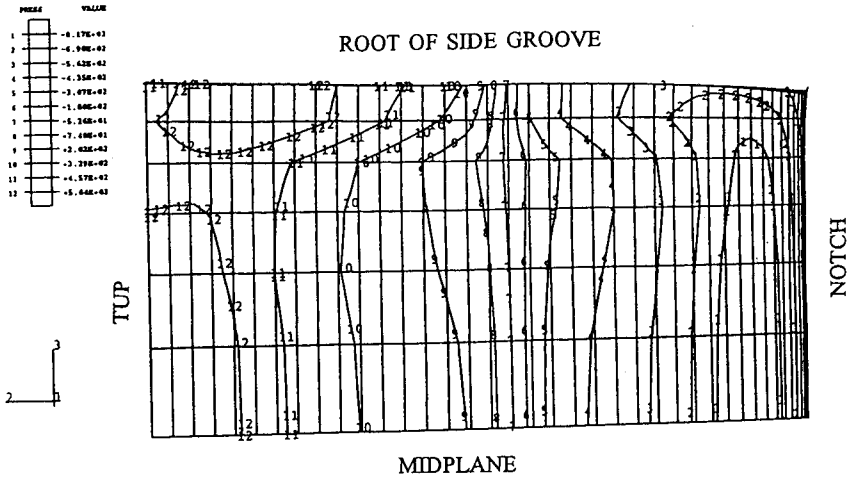

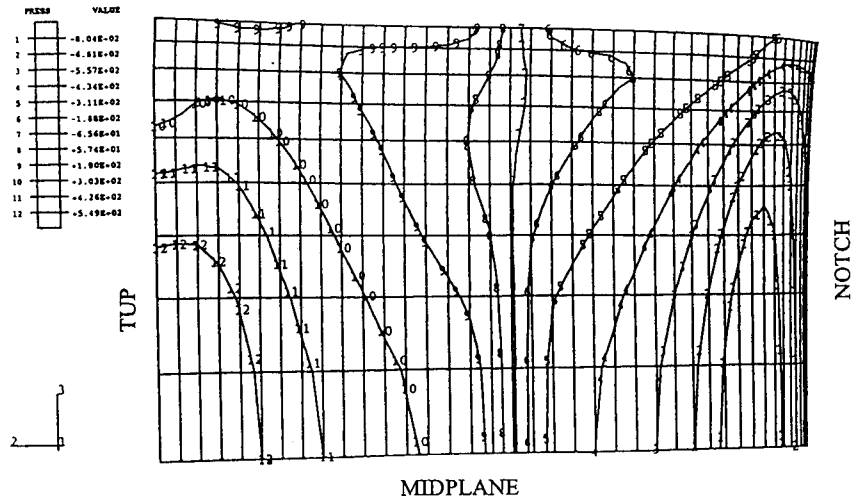

FIG. 10--Comparison of fracture plane hydrostatic pressure contours at a displacement of 1.5 mm for notched specimens both with (top) and without (bottom) side grooves

stress field in the miniature specimen without side grooves extends along the notch to half the distance of the conventional specimen. This relative increase in the peak stress region size due to size grooves is expected to reduce scatter (and therefore less specimens will be needed) for specimens tested in the transition region where the trigger particle mechanism dominates brittle fracture initiation.

Striker Design and Contact Conditions

In our recent finite element study, which was focused on non-linear response prior to crack initiation, two sensitivity studies related to tup design were performed. The first study compared the load versus deflection behavior from the ISO and ASTM tup designs. For loading up to displacements representative of peak Charpy test loads, the ISO tup was found to result in load levels that were about 5% below those of the ASTM tup. This load decrease was attributed to the fact that the relatively flat contact region of the ASTM tup is about 10% of the support span width. This flat contact region results in the contact forces being significantly concentrated near the ends of the contact region. This concentration, in effect, results in a four point bending condition. If the contact forces were exactly concentrated at the corners, the applied moment for a given load level would be 10% less than for the three point bending condition. The smaller 5% effect that was observed in the finite element simulation is easily accounted for by the fact that contact forces, while peaked at the corners, do exist all along the contact region.

In the second finite element sensitivity study, the ASTM tup design was used with two levels of friction. In one case, the friction coefficient was zero while in the other, the coefficient was 0.5. In the latter case, the maximum friction force was further limited by the shear yield strength of the specimen material. Since the frictional forces were observed to be largely limited by this yield stress value, the assumed coefficient had little effect on the results. The calculations showed that the addition of frictional forces increased the applied load levels by about 10%. This load increase was attributed to frictional forces at the support points restraining the longitudinal expansion of the notched side of the specimen.

Both of these results are consistent with several experimental observations that have appeared in the literature for which the sum of the Charpy energies for the two tup geometries have been compared. Tower [19] showed that different Charpy energies can result from using the ISO and the ASTM tups when testing highly ductile materials. While for energy levels below 60 J, differences were negligible, for energies in the 100 to 200 J range, energies were as much as 25% larger for the ASTM tup. The explanation given for this increase in energy was the intense localized deformation caused by the corners of the ASTM tup design. These corners allowed the tup to essentially gouge the contact surface as the result of the contacted surface of the specimen wanting to contract under the bending induced compression at this surface. This gouging action results in significant plastic deformation and energy dissipation. While the higher Charpy energy levels of the Tower study were for materials other than vessel steels, similar behavior with energy differences in the 10 to 15% range have been observed for nuclear pressure vessel steels on the upper shelf [11].

By restricting the contraction of the specimen's contacted surface, the ASTM tup results in a net tensile stress being superimposed on the fracture plane bending stress distribution. This additional tension might be expected to decrease the chance that a specimen will wrap around the tup rather than break into two pieces. This behavior has been observed by researchers at the Belgian Nuclear Research Center [20]. It is not clear how this superimposed tensile stress would be

reflected in the Charpy energy differences since the higher loads of the ASTM design would be truncated at the time of separation while the lower load levels of the ISO design would continue until the specimen slips off the supports.

Some direct evidence exists for the contact surface gouging being the primary cause of the higher energies for the ASTM tup design. In their specimen reconstitution work, Belgian Nuclear Research Center researchers have found that localized hardening due to welding near the tup contact region can reduce the degree of gouging [21]. When the gouging is avoided, the ISO and ASTM tups result in esentially the same Charpy energies. To further confirm this conclusion that the gouging and higher energies are linked, tests were done in which a hard tungsten foil was placed between the ASTM tup and the specimen. Again the gouging was avoided, and the Charpy energies were essentially the same as those from using the ISO tup design.

With the above observations, it was decided that our miniature specimen testing program would focus on using the ISO tup design. One reason for this choice is that the energy that one obtains from a Charpy test is intended to be indicative of the fracture resistance of the material. The fact that a part of the energy obtained from some tests using the ASTM tup design is totally unrelated to the fracture process is seen as an unattractive feature. Perhaps the more compelling reason is that miniature specimens will tend to behave in a more ductile manner than full scale specimens therefore tending to exaggerate this undesireable gouging behavior in the miniature specimens. If there is a negative side to using the ISO tup in the miniature specimen testing, it is probably that there may be a greater chance that the specimen will not fracture to the point of becoming two pieces. This behavior would be expected to be more likely for the miniature specimens than full size specimens due to the relatively more ductile behavior of the smaller specimen.

Inertial Effects

Figures 11 and 12 show the results of two dynamic analyses. Both analyses assume plane strain conditions. Quasi-static stress-strain properties were used for these simulations. The data presented in Figure 11 is for a constant tup velocity of 3 m/sec which is the low end of the tup velocity range stipulated by the ASTM standard E23. Figure 12 resulted from assuming a constant tup velocity of 6 m/s, the upper end of the stipulated velocity range. The load-deflection curves from the static analyses are included in these plots for comparison with the dynamic curves. For the static loading case, the tup and anvil loads are equal (but in opposite directions). This is not generally the case for the dynamic analysis due to the inertial effects and therefore both loads are plotted. It can be seen that the tup and anvil loads tend to be out of phase with respect to each other. For earlier times (small deflections), the oscillation of the loads is very large. However, once plastic deformation becomes significant, the high frequency oscillations are quickly damped out. Another factor which contributes to the dynamic behavior approaching quasi-static loading behavior is that the loading rate is relatively slow compared to the stress wave speeds. Elastic stress wave speeds are between 3×10^6 mm/sec and 6×10^6 mm/sec depending on the type of wave (compressive, shear, or surface). At this speed, stress waves can propagate to the end of the specimen and return to the notch region 25 to 55 times by the time the tup displaces the specimen 3 mm.

Examining the right side plots of Figures 11 and 12, it can be seen that the anvil does not exert a reaction until a tup displacement of about 0.04 or 0.08 mm. This reflects the time that it takes for the stress wave from initial contact to propagate to the anvil contact

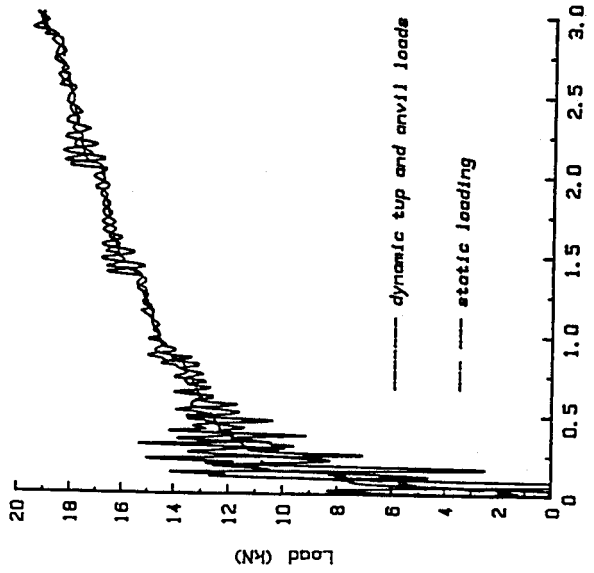

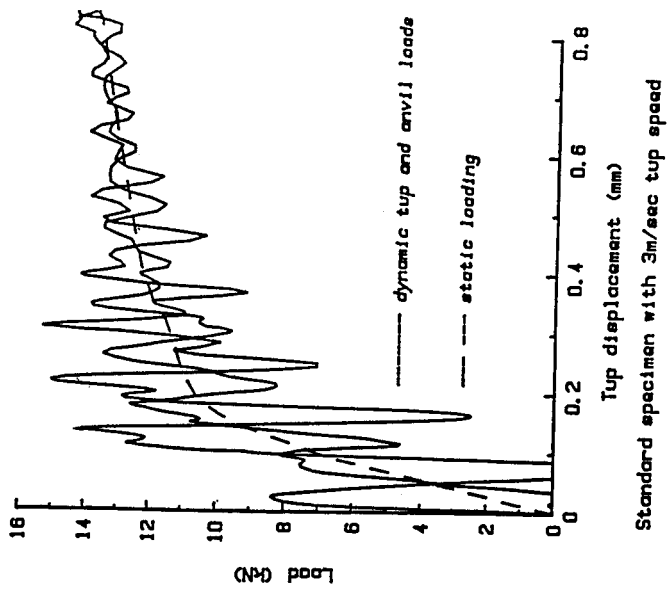

FIG. 11--Dynamic load versus tup displacement behavior for the standard specimen being struck with a tup speed of 3 m/sec

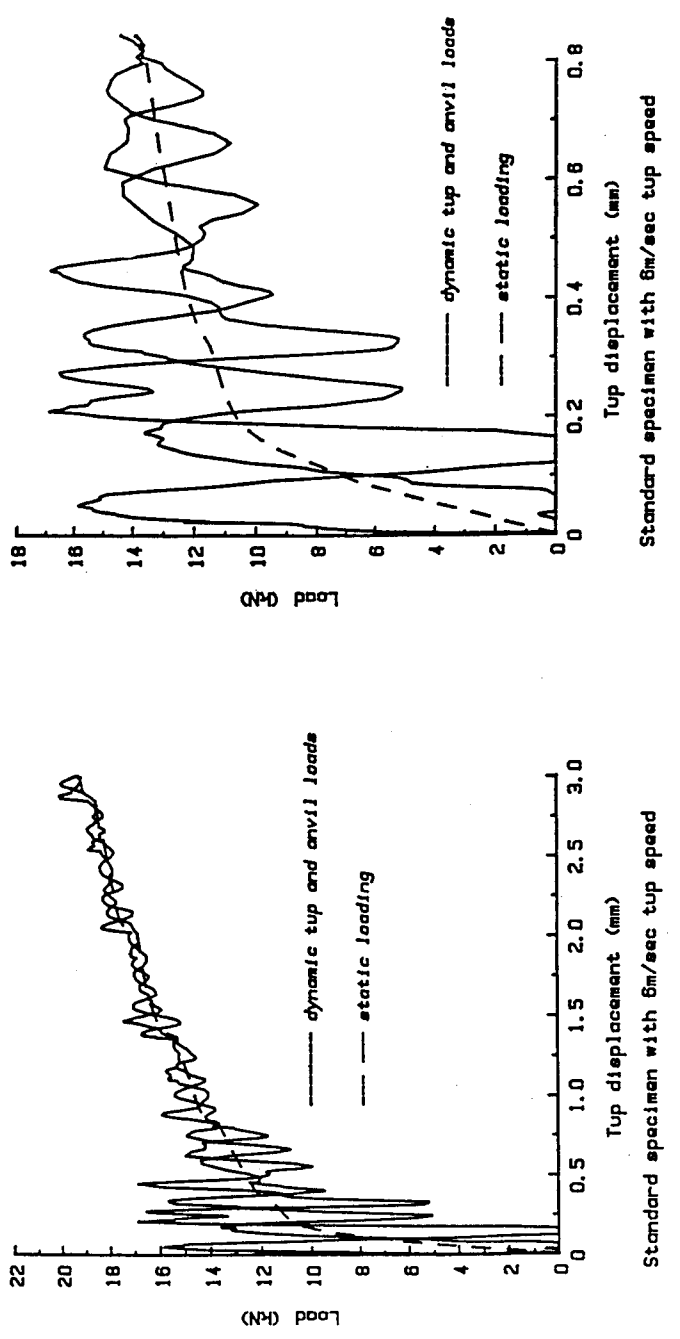

FIG. 12--Dynamic load versus tup displacement behavior for the standard specimen being struck with a tup speed of 6 m/sec

location. These plots also show that the first oscillation in the tup load results in the tup load going to zero for a period of time. This is the result of the specimen springing away from the tup shortly after initial contact. This springing away is the result of the first stress wave returning to the tup contact region after having reflected from the end of the specimen.

It is worth noting that the size of the tup load oscillations found in these dynamic simulations are larger than typically measured during instrumented Charpy testing. The fact that the size of the oscillations obtained experimentally seem to depend to some extend on the group doing the work suggests that perhaps "electrical damping" in the measurement systems may be a partial explanation. In fact, many researchers have used signal conditioners which operate in the few tens of kHz range. Our calculations show that the load transducer signal is in the 20 to 40 kHz range. Therefore, a system capable of at least 100 kHz, with a 1 MHZ sampling rate, is needed to accurately determine the general yield load.

To verify scalability of the full size dynamic Charpy solution to a half size specimen, a half scale version of the coarse 2D grid was generated. All dimensions, including those of the tup and anvil, were halved. For static loading, the stress and strain solution scaled exactly with that of the full scale model. The dynamic simulation, run with a tup velocity of 6 m/sec, verified that the dynamic solution also scales exactly if both specimen sizes are impacted with tups having the same velocity. The principal conclusion to be drawn from this analysis is that the tendency for inertial effects to become negligible after general yield also occurs for the half scale specimen.

Weld Reconstitution

The effect of weld reconstitution was simulated using a refined 2D plane strain model of a standard Charpy in which the weld and heat affected zones were given a yield stress 20% above the base metal value. The elevated yield stress was applied to a region that extended from 4 mm to 6 mm from the specimen's fracture plane. The model was then loaded to a deflection representative of peak load values for upper shelf behavior. It was found that the plastic zones emanating from the notch and the tup contact region reached the high yield region even before general yield. This interaction resulted in a strain increase at the notch relative to that in an unwelded specimen. This strain increase was nearly 15% for displacements representative of peak load conditions. If crack growth behavior is strain controlled, this suggests that Charpy energies in the reconstituted specimen could be reduced by about 15%.

Figure 13 shows the extent of the plastic zones in a Charpy specimen as a function of applied load and as a function of applied displacement. Normalizing the load by general yield load makes the results applicable to other yield stress levels. Normalizing plastic zone size and applied deflection by the specimen height allows the results to be applied to specimens of nonstandard size. It can be seen that the plastic zone extent tends to peak at about one specimen height. This strongly suggests that the minimum distance that a weld should be from the fracture plane is about one specimen height. With half scale specimens, this would enable a change of material orientation in the reconstituted specimens.

TEST GEOMETRY RECOMMENDATIONS FOR RPV STEELS

Microstructural considerations resulted in the proposed specimen cross-sectional dimensions being set at half of the standard Charpy

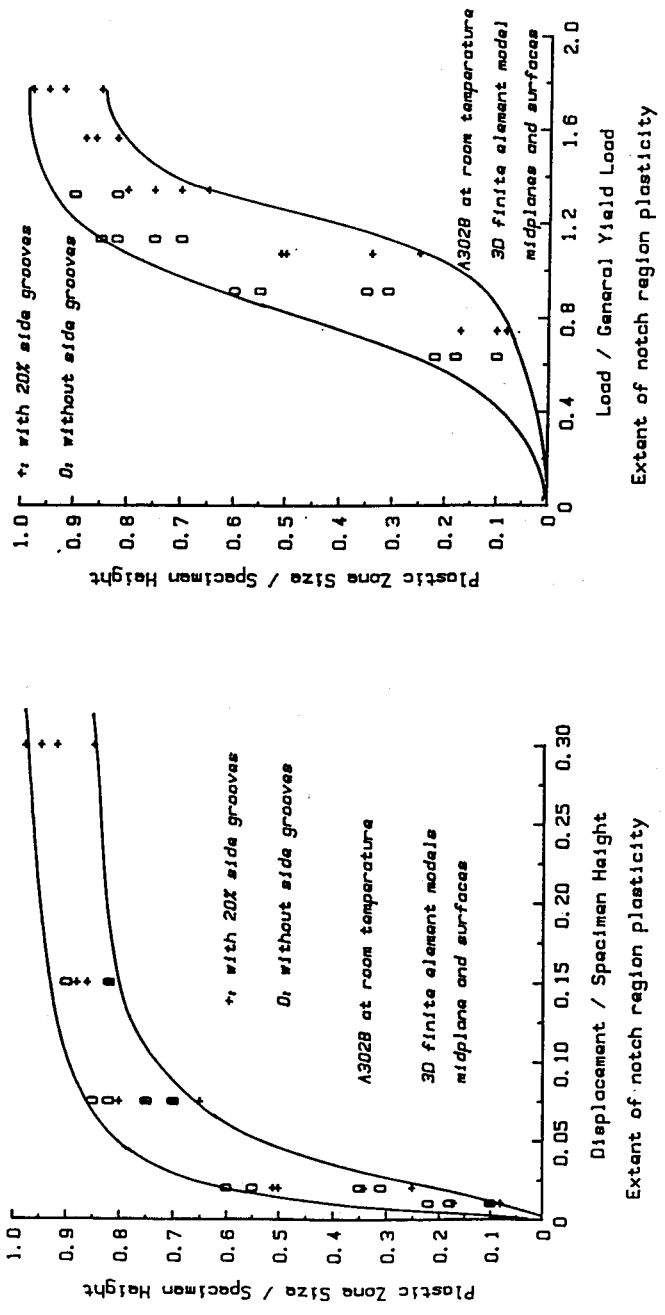

FIG. 13--Summary of plastic zone size results from 3D finite element simulations of Charpy specimens

specimen dimensions. Therefore the miniature specimen cross-section is 5 mm by 5 mm. It was determined that scaling the length of the miniature specimen so as to maintain the same bending-to-shear ratio as the standard specimen would be best. This decision was based in part on the fact that miniature specimens will require relatively higher load levels than full scale specimens which could have adverse effects if a shortened design were selected. The only disadvantage of not using a shorter design is that fewer specimens can be made from a single broken Charpy specimen. However, it is believed that this can be overcome by the use of weld reconstitution. To the extent that it is the spacing between the support points which determined the bending-to-shear stress ratio, the miniature specimens can be slightly shorter than half scale provided that the half scale of the support spacing is maintained.

Although it is possible that keeping the same bending-to-shear ratio as for the full size specimen (i.e., span-to-depth ratio) could have prevented the plastic collapse type miniature specimen failures observed in previous work, the use of side grooves is still highly advantageous. Although both full size and miniature specimens have plane strain fields over a significant portion of their notch or crack fronts, the portion of the front with plane strain behavior tends to decrease with increasing plasticity. The use of side grooves greatly increases the percentage of the notch or crack front that exhibits plane strain behavior. This is particularly important for small specimens since fracture behavior is known to depend on the size of the region that is subjected to critical stress levels. By maximizing the plane strain zone of the miniature specimen, the fracture behavior should be more like that of a larger specimen. This relatively larger plane strain zone size should therefore also tend to reduce experimental scatter such as might be expected for a smaller specimen size.

It was concluded that relatively standard side grooves are appropriate (20% of thickness, 0.2 to 0.4 mm radius, 45° angle). Using deeper side grooves than 20% would be expected to result in a net decrease in the absolute size of the notch or crack region with plane strain behavior as the result of reducing the total notch front length. Using shallower side grooves would be expected to provide less satisfactory stress field improvement at the higher load levels. Using a larger groove angle would tend to reduce the side groove effectiveness by reducing the intensity of the stress field induced by the side groove. Decreasing the side groove angle would tend to increase the intensity of the side groove stress field and possibly provide slightly better performance in terms of the notch tip fields, but could lead to side groove closure on the compression side of the specimen which would result in discontinuous specimen stiffness behavior.

The use of side grooves is likely to decrease or eliminate the tendency for ductile fracture (shear lips) near the surfaces of the specimen. This might be expected to shift the Fracture Appearance Transition Temperature (FATT) to higher temperatures by reducing the percent shear at a given temperature. This reduction in shear lip formation would also seem to result in less resistance to a dynamically propagating crack; thus again tending to promote a decrease in the percent ductile fracture evaluation. (It seems likely that tunneling associated with cleavage crack growth in specimens without side grooves results in plastic dissipation of energy that would otherwise be available for cleavage.) These effects would tend to increase the FATT, making results more conservative, and would therefore be expected to reduce any correction needed to relate the miniature specimen results to full scale specimen results.

The above described 2D and 3D, large deformation, finite element analyses have shown that plane strain conditions exist over a significant portion of the standard specimen notch for loads up to those

representative of upper shelf behavior. For loads below general yield (lower shelf), about 3/4 of the notch tip is reasonably close to the 2D plane strain solution. As loads approaching those for upper shelf fracture behavior are applied, the portion of the notch exhibiting plane strain behavior decreases to about 1/4 of the total notch length. Adding 20% side grooves greatly reduces the loss of plane strain at the higher load levels. At load levels representative of upper shelf behavior, the side grooved geometry retains plane strain behavior over about 1/2 of the notch front. For a half scale specimen, the absolute length of plane strain along the notch is then 1/2 x 80% x 5 mm = 2 mm. For the full scale specimen, the plane strain region is 1/4 x 10 mm = 2.5 mm. Therefore the side grooves significantly offset the absolute reduction in the plane strain notch front region.

A 2D simulation of a weld reconstituted specimen showed that if the weld is too close to the fracture plane, the presence of the weld can induce larger plastic strains in the fracture process zone for a given applied displacement level. This increase in the fracture process zone strain intensity for a given applied displacement can be expected to reduce Charpy energy levels. This is consistent with available experimental results [22][23]. This weld reconstitution simulation, when combined with plastic zone size information from the 3D simulations of this study, allow a smallest weld insert size to be determined. The plastic zones in the 3D models were observed to extend as far as one specimen height from the fracture plane. Since any interaction between the weld heat affected zone and the fracture region plastic zone could result in the weld affecting the specimen behavior, this means that the weld and its heat affected zone should be no closer to the fracture plane than one specimen height.

A study of tup design effects on measured Charpy energies showed that the difference between the ASTM standard tup geometry and the ISO tup geometry is negligible except when very ductile materials are being tested [19]. This increase in energy is mainly associated with the corners of the ASTM tup gouging the contact surface of the specimens when large deformations are required to break the specimens. Since the miniature specimens will tend to require relatively larger deflections than the full scale specimens, it is judged that the ISO tup design is preferable.

Scaling the ASTM anvil (support) radius and spacing appears most appropriate for the miniature specimen testing. Scaling the spacing will result in equal bending-to-shear load ratios for full scale and mini specimens. Scaling the support radius should result in similar behavior for both size specimens.

Inertial effects (i.e., stress wave effects) tend to become insignificant after general yield load is reached due to the damping associated with plastic deformation. Experimental results show that general yield conditions are attained prior to crack growth throughout the transition temperature range [4, 16]. General yield occurs at an energy level of about 3 or 4 J (standard Charpy). The tendency for higher load levels in mini specimens relative to the general yield load should make inertial effects even less significant.

Strain rate effects associated with impact testing (as opposed to quasi-static testing) are significant for both full scale and mini specimens. Though strain rates in a half scale miniature specimen will be twice those of a full scale specimen if equal impact speeds are used, this change in strain rate is expected to have negligible effects on specimen behavior. This is because strain rate effects enter primarily though the elevation of yield stress and a doubling of strain rate increases the yield stress by only a couple percent.

Finite element analysis as well as dimensional analysis has shown that stress and strain states in the miniature specimen can simulate those in a full scale specimen provided proper scaling is applied. However, it has also been shown that load and displacement levels required to induce fracture will be relatively higher in the miniature specimen (e.g., compared to those at general yield). Before correcting for the load reduction associated with the use of side grooves, load levels would be expected to be about 5 to 10% larger in the half scale miniature specimen. Displacement levels could be 80 to 90% larger. Energies can be expected to be between 1/8 and 1/4 of those for full scale specimens.

SUMMARY AND CONCLUSIONS

Design of all miniature specimens should begin with a thorough examination of the material microstructure to determine the minimum specimen dimension. In the case of the MNT, the proposed minimum cross section dimension is 5 mm x 5 mm for RPV materials to ensure that chemical bands and inclusion stringers within the steel are adequately represented. In order to simulate the stress state of the conventional specimen, a 1/2 scale factor has been proposed. The 1/2 scale factor applies to the specimen dimensions as well as to the span and tup radius. In addition to scaling the key test parameters, 20% side grooving is recommended to substantially increase the volume of material which is exposed to plane strain conditions. Miniature specimens tested on the upper shelf which are side grooved will produce an absolute length of plane strain along the notch which is about 80% of that experienced in conventional 10 mm x 10 mm x 55 mm specimens. Therefore, side grooves will significantly offset the reduction in plane strain at the notch/crack tip for miniature specimens.

Generally, it is expected that a smaller specimen will tend to behave as though the material is tougher. This is the fundamental result of the nonscalability of the material microstructure and the mathematics associated with singular crack tip fields. In terms of transition temperature behavior, this means that the transition temperature measured with a smaller specimen will tend to be lower than the transition temperature measured with a larger specimen. The design of the miniature specimen has focussed on minimizing this shift. The most significant design aspects in terms of reducing this shift are the side grooves, and the use of proportional scaling. Basically, the side grooves will make the smaller specimens behave as though the material is less tough, as compared to the behavior that would be obtained if a perfectly scaled Charpy geometry were used.

Although the feasibility preparing 16 miniature specimens from the broken halves of one conventional specimen has been experimentally demonstrated, detailed analysis of the miniature specimen stress fields has shown that the conventional specimen aspect ratio results in a favorable bending-to-shear ratio. The larger aspect ratio limits the number of specimens which can be machined from a conventional specimen to 8 (4 from each broken half). However, the larger miniature specimens have the significant advantage that they can be weld reconstituted since the requirement of providing an insert of 4 times the width (W) can be satisfied. Therefore, it is now possible to produce 24 miniature specimens (as opposed to 16 earlier) from one conventional specimen using the weld reconstitution procedure. This strategy is particularly effective in nuclear reactor pressure vessel surveillance in cases where a limited fixed volume of material is available. A surveillance capsule can be withdrawn, the specimens tested, and 8 miniature specimens can then be machined from the broken halves of each specimen. Then, after further irradiation, the specimens can be tested and weld reconstituted to produce an additional 24 specimens for re-irradiation and testing.

Thus, using this strategy, it will be possible to produce sufficient data for accurate trend curve development on a plant-specific basis.

ACKNOWLEDGMENT

The authors are grateful to the Empire State Electric Energy Research Corporation (ESEERCO) and the New York state utilities for their sponsorship of this work. We are also grateful to Dr. L.J. Cuddy (Metallurgical Consultants) for his technical assistance with the microstructural work. We also wish to thank Mr. A.J. Peterson for his recognition of the importance of this work and his efforts in championing the technology.

REFERENCES

[1] Lucas, G.E., Odette, G.R., Sheckherd, J.W., McConnell, P., and Perrin, J., "Subsized Bend and Charpy V-Notch Specimens for Irradiated Testing", The Use of Small-Scale Specimens for Testing Irradiated Material, ASTM STP 888, W.R. Corwin and G.E. Lucas, Eds., American Society for Testing and Materials, Philadelphia, 1986, pp. 305-324.

[2] Corwin, W.R. and Hougland, A.M., "Effect of Specimen Size and Material Condition on the Charpy Impact Properties of 9Cr-1Mo-V-Nb Steel", The Use of Small-Scale Specimens for Testing Irradiated Material, ASTM STP 888, W.R. Corwin and G.E. Lucas, Eds., American Society for Testing and Materials, Philadelphia, 1986, pp. 325-338.

[3] Harling, O.K., Lee, M., Sohn, D-S., Kohse, G., and Lau, C.W., "The MIT Miniaturized Disk Bend Test", The Use of Small-Scale Specimens for Testing Irradiated Mateiral, ASTM STP 888, W.R. Corwin and G.E. Lucas, Eds., American Society for Testing and Materials, Philadelphia, 1986, pp. 50-65.

[4] Manahan, M.P. and Charles, C., "A Generalized Methodology for Obtaining Quantitative Charpy Data From Test Specimens of Nonstandard Dimensions", Nuclear Technology, Vol. 90, May 1990.

[5] "Small Specimen Test Techniques Applied to Nuclear Reactor Vessel Thermal Annealing and Plant Life Extension", American Society for Testing and Materials, ASTM STP 1204, October, 1993.

[6] Rosinski, S.T., Kumar, A.S., Cannon, N.S., and Hamilton, M.L., "Application of Subsize Specimens in Nuclear Plant Life Extension", Small Specimen Test Techniques Applied to Nuclear Reactor Vessel Thermal Annealing and Plant Life Extension, ASTM STP 1204, W.R. Corwin, F.M. Haggag, and W.L. Server, Eds., American Society for Testing and Materials, Philadelphia, 1993, pp. 405-416.

[7] Kumar, A.S., Louden, B.S., Garner, F.A., and Hamilton, M.L., "Recent Improvements in Size Effects Correlations for DBTT and Upper Shelf Energy of Ferritic Steels", Small Specimen Test Techniques Applied to Nuclear Reactor Vessel Thermal Annealing and Plant Life Extension, ASTM STP 1204, W.R. Corwin, F.M. Haggag, and W.L. Server, Eds., American Society for Testing and Materials, Philadelphia, 193, pp. 47-61.

[8] Hamada, J., Sato, S., and Kohyama, A., "Fracture Toughness Evaluation of Neutron-Irradiated Composites by a Miniaturized Charpy Test", Small Specimen Test Techniques Applied to Nuclear Reactor Vessel Thermal Annealing and Plant Life Extension, ASTM STP 1204, W.R. Corwin, F.M. Haggag, and W.L. Server, Eds., American Society for Testing and Materials, Philadelphia, 1993, pp. 77-89.

[9] Kryukov, A.M. and Sokolov, M.A., "Investigation of Material Behavior Under Reirradiation After Annealing Using Subsize Specimens", Small Specimen Test Techniques Applied to Nuclear Reactor Vessel Thermal Annealing and Plant Life Extension, ASTM STP 1204, W.R. Corwin, F.M. Haggag, and W.L. Server, Eds., American Society for Testing and Materials, Philadelphia, 1993, pp. 417-423.

[10] Amayev, A.D., Badanin, V.I., Kryukov, A.M., Nikolayev, V.A., Rogov, M.F., and Sokolov, M.A., "Use of Subsize Specimens for Determination of Radiation Embrittlement of Operating Reactor Pressure Vessels", Small Specimen Techniques Applied to Nuclear Reactor Vessel Thermal Annealing and Plant Life Extension, ASTM STP 1204, W.R. Corwin, F.M. Haggag, and W.L. server, Eds., American Society for Testing and Materials, Philadelphia, 1993, pp. 424-439.

[11] van Walle, E., Fabry, A., Van de Velde, J., Chaouadi, R., Puzzolante, J.L., Van Ransbeeck, T., "Pressure Vessel Steel Programme at the Belgian Nuclear Research Centre", March 8, 1993.

[12] Manahan, M.P., Williams, J., and Martukanitz, R.P., "Laser Weld Reconstitution of Conventional Charpy and Miniaturized Notch Test (MNT) Specimens", Small Specimen Test Techniques Applied to Nuclear Reactor Vessel Thermal Annealing and Plant Life Extension, ASTM STP 1204, W.R. Corwin, F.M. Haggag, and W.L. Server, Eds., American Society for Testing and Materials, Philadelphia, 1993, pp. 62-76.

[13] Manahan, M.P., "Determination of Charpy Transition Temperature of Ferritic Steels Using Miniaturized Specimens", Journal of Materials Science 25 (1990) 3429-3438.

[14] Manahan, M.P., "Determination of Fracture Behavior of Ferritic Steels Using Miniaturized Specimens", Journal of Nuclear Materials 166 (1989) 321-330.

[15] Cheverton, R.D., Bolt, S.E., Ball, D.G., Iskander, S.K., Nanstad, R.K., "Pressure Vessel Fracture Studies Pertaining to the PWR Thermal-Shock Issue: Experiments TSE-5, TSE-5A, and TSE-6", NUREG/CR-4249, June, 1985.

[16] Rolfe, S.T. and Barsom, J.M., Fracture and Fatigue Control in Structure, Prentice-Hall, Englewood Cliffs, NJ, 1977.

[17] Flemings, M.C., Solidifcation Processing, McGraw-Hill, 1974, p. 149.

[18] Green, A.P. and Hundy, B.B., "Initial Plastic Yielding in Notched Bend Tests", Journal of the Mechanics and Physics of Solids, Vol. 4, No. 2, March 1956, pp. 128-144.

[19] Towers, O.L., "Effects of Striker Geometry on Charpy Results", Metal Construction, 1983, 15(11).

[20] Private communication, M.P. Manahan, MPM Research & Consulting, and E. van Walle, SCK/CEN, 1994.

[21] van Walle, E., Fabry, A., Van Ransbeeck, T., Puzzolante, J-L., Vandermeulen, W., Van de Velde, J., "The Reconstitution of Small Remnant Parts of Charpy-V Specimens", presented at SMIRT 11, PCS II, Taipei, Taiwan, August 1991.

[22] van Walle, E., Van Ransbeeck, T., Chaouadi, R., A. Fabry, Puzzolante, J.L., Vandermeulen, W., and Van de Velde, J., "The Reconstitution Effort at SCK/CEN", SCK/CEN Research Group Materials, 1993.

[23] Fabry, A., Puzzolante, J.L., Van Walle, E., Vandermeulen, W., Vandevelde, J., and Van Ransbeek, T., "Changing the Notch Orientation of Charpy-V Specimens by Stud Welding of Broken Remnants", Work performed on Request of Yankee Atomic Electric Company.